

# Ordering and Dynamics of Vibrated Hard Squares

Lee Walsh<sup>1</sup> and Narayanan Menon<sup>1,2</sup>

<sup>1</sup>Department of Physics, University of Massachusetts, Amherst, USA

<sup>2</sup>TIFR Centre for Interdisciplinary Science, Hyderabad, India

E-mail: lawalsh@physics.umass.edu, menon@physics.umass.edu

**Abstract.** We study an experimental system of hard granular squares in two dimensions, energized by vibration. The interplay of order in the orientations and positions of anisotropic particles allows for a rich set of phases. We measure the structure and dynamics of steady states as a function of particle density. This allows us to identify a progression of phases in which a low density isotropic fluid gives way to a phase with tetratic orientational order, short-range translational correlations, and slowed rotational dynamics. In this range of density we also observe a coupling between the orientational order and bond-orientational order. At higher densities, the particles freeze into a translationally and orientationally ordered square crystalline phase in which translational diffusion is suppressed.

**Keywords:** granular matter, phase diagrams (experiments), jamming and packing, driven diffusive systems (experiments)

## 1. Introduction

An assembly of hard squares in two dimensions presents a variety of potential spatial orders. Hard particles form thermodynamic phases dictated solely by the entropy of their geometric packing; temperature is irrelevant as the interaction potential has no finite energy scale. Particles with asymmetric shapes have anisotropic constraints of self-avoidance and therefore pack in complex phases. Squares are an obvious point of entry into this complexity because they can tile the plane without frustration. However, there has been relatively little investigation into the phases formed by this simple shape as a function of density, and still less of the dynamics within these phases.

Interesting phase behavior in two dimensions does not require anisotropic shapes: the phase diagram of isotropic hard disks is an important paradigm in statistical physics [1–3] and offers a context for the ordering of asymmetric particles. A two-dimensional crystal of disks has algebraic (power-law) correlations in particle positions. This melts into a phase in which the orientation of “bonds” between neighboring particles have long-range correlations, which at even lower density finally melts into an isotropic phase.

Anisotropic particles have both translational and rotational degrees of freedom, each of which may order independently. This additional degree of freedom provides the

possibility of new classes of order. For example, particle orientations may order independently of their locations, giving rise to phases with global orientational order in the absence of translational order. The most widely known of such phases is the nematic liquid crystal phase, in which the molecular orientations are mutually aligned while the locations are disordered. These phases in two dimensions have been explored using various rigid shapes with a two-fold rotational symmetry, such as rectangles [4,5], ellipses [6], or rods [7–9]. Some of these two-fold symmetric particles yield phases with four-fold symmetry. This has also been demonstrated by density functional theories [10,11]. Minor differences in shape can have drastic effects on the phase diagram of such systems in two dimensions [12–14], and three dimensions [15–17].

Existing work on shapes with four-fold symmetry — such as squares — is limited, but raises interesting questions about the phase diagram. Monte Carlo simulations of an equilibrium hard-square system by Wojciechowski and Frenkel suggest a four-fold tetratic phase with longer-range orientational order than translational order [18]. By contrast, in experiments on a colloidal suspension of square-shaped tiles osmotically constrained to a surface, Zhao *et al.* found no evidence of an orientationally ordered state [19]. At densities above that of the isotropic phase, they instead observed a hexagonal rotator phase where particles have the translational order of a hexagonal lattice but no orientational correlation. At higher densities, the system enters a rhombic phase with a lattice angle that continuously approaches the  $90^\circ$  angle of a square crystal at full packing.

Particle shape is the critical difference between these two studies: the simulation uses perfect squares, while the experimental particles have rounded corners. The effect of rounding the corners was investigated through Monte Carlo simulations by Avendaño and Escobedo [12]. They found that squares with sufficiently rounded corners form the hexagonal rotator phase observed by Zhao, *et al.* [19], but that squares with sharper corners instead pass through a tetratic phase before crystallizing, as in the simulations by Wojciechowski and Frenkel [18].

Consequently, experimental evidence for the phase behavior of hard squares is needed. Furthermore, individual particle dynamics can be measured via experiment, which Monte Carlo simulations do not capture. In this work we present experimental observations of structure and translational and rotational dynamics of the steady states of a system of vibrated hard granular squares. The macroscopic nature of the system gives us the advantage of precise control over the particle properties, including shape [8,20–22]. However, our system size is necessarily small, though comparable to previous simulations and experiments [9,12,18,19]. As a result, transitions are rounded off due to finite number, and truly long-range correlations are truncated by the boundary.

We find a progression from an isotropic disordered fluid at low density, through a fluid with increased orientational order, arriving at a solid with both orientational and translational order. The intermediate orientational order is tetratic, and no hexagonal rotator or rhombic phases are seen. The static structure analysis gives qualitative agreement with Monte Carlo simulations [12,18]. We also present new results on the dynamics of particles as a function of density. We find that rotational diffusion is suppressed relative to translational diffusion in the approach to the tetratic phase. The transition to the solid is marked by the loss of translational diffusion.

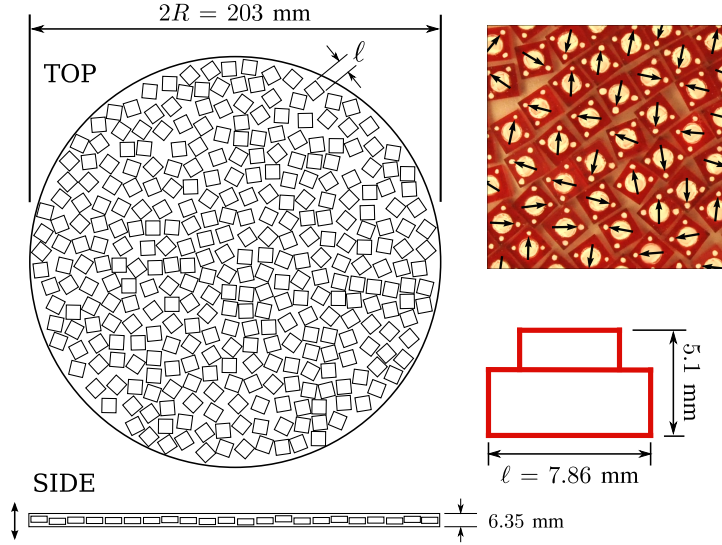


**Figure 1.** Experimental setup: Particles ( $N \approx 500$ ) are constrained in a quasi-two-dimensional circular dish between an aluminum substrate and acrylic cover. The dish has diameter  $2R = 203 \text{ mm}$  with height  $6.35 \text{ mm}$ , and particles have side length  $\ell = 7.86 \pm 0.01 \text{ mm}$  and height  $5.1 \text{ mm}$ . Photo at upper right shows the particles (at density  $\rho = 0.73$ ) painted with white tracking targets at center and three corners. Arrows show location and orientation of detected particles.

## 2. Experiment

We confined square particles to a monolayer in a horizontal dish. Vertical vibration provides quasi-thermal noise in two dimensions and the particles diffuse in plane. The setup is shown in figure 1. Particles are hard plastic tiles (manufactured by LEGO) with sides of length  $\ell = 7.86 \pm 0.01 \text{ mm}$  and base height of  $3.2 \text{ mm}$ , plus a  $1.9 \text{ mm}$  high cylindrical protrusion on the top, for a total height of  $5.1 \text{ mm}$ . Corners have radius of curvature  $\sigma/2 = 0.15 \pm 0.01 \text{ mm}$ , giving a corner-rounding-to-length ratio  $\zeta = \sigma/\ell = 0.04$  [12]. Their mass is  $204 \pm 1 \text{ mg}$ . The particles are contained in a circular aluminum dish of diameter  $2R = 20.3 \text{ cm}$  with an acrylic lid that maintains a vertical gap of  $6.35 \text{ mm}$  (1.25 particle height). The dish is coupled to a permanent magnet electrodynamic shaker (LDS V456 shaker and PA1000L amplifier), which vibrates the dish vertically following sine-wave motion with peak acceleration  $\Gamma \approx 10g$  at frequency  $f = 50 \text{ Hz}$ .

Particles were imaged from above with a high-speed camera (Vision Research Phantom v7.1) to measure displacements, and a DSLR camera (Nikon D5000) to measure positions. They are marked with dots for detection of position and orientation, as shown in figure 1. For dynamic measurements, we uniquely identified and tracked particles through 120-fps video. Positional uncertainty, primarily from lighting and imaging, is  $0.25$  pixels, which corresponds to  $0.01\ell$  in videos and  $0.002\ell$  in stills, where  $\ell$  is the particle size. For all data, orientational uncertainty is  $0.02 \text{ rad}$  and is dominated by inaccuracy in marking dot location.

We controlled the density (packing fraction)  $\rho = N\ell^2/\pi R^2$  by varying the number of particles  $N$  in the dish. At the boundary, particles tend to align with the dish walls, therefore all particles within a margin of width  $2\ell$  of the boundary are excluded from the analysis and density calculations. The flux of particles into and out of the excluded region leads to fluctuations of  $\pm 0.005$  about the reported densities.

In this nonequilibrium system, energy is fed to particles via collisions with the vibrating cell. Collisions between particles and the bottom plate, the lid, and other particles are inelastic, and kinetic energy is dissipated quickly. Likewise, momentum of the particles is not conserved due to collisions and friction with the substrate. However, the nonequilibrium drive from the vertical vibration provides noise that leads to motion in the horizontal direction. The conversion from vertical forcing to horizontal dynamics is mediated by the detailed mechanics of the particle-substrate collision; however, the symmetry of the resultant driving force on the particle matches the symmetry of the particle shape. At very short timescales, on the order of the vibration period  $1/f$ , the dynamics may reflect this symmetry, but the motion of the tiles is isotropic at longer timescales.

### 3. Structure

In this section, we study the emergence of ordered phases by capturing static images of the system over a range of densities. The images were taken at time intervals (minutes) long enough compared to typical diffusion times (seconds) to obtain statistically independent configurations of the particles. We characterized spatial order with order parameters and correlation functions computed from particle positions and orientations.

#### 3.1. Positional Order

We first consider translational order by studying particle positions, regardless of their orientations. Translational order can be quantified by the radial distribution function  $g(r)$ , which gives the probability density of finding two particles separated by distance  $r$ . Our measurement is shown in figure 2. As density increases, we observe sharper and taller peaks; the peaks are asymmetric, with sharp lower bounds at integer values of  $r/\ell$ , which correspond to particle separation in a perfect square packing. At the highest two densities ( $\rho > 0.82$ ), a peak forms near  $r/\ell = \sqrt{2}$ , corresponding to the second-nearest neighbor in a square crystal.

The characteristic length of translational order can be determined from the functional form and length scale of the decay envelope of  $g(r)$ . Short-range order is associated with exponential decay  $e^{-r/L}$ , while quasi-long-range order is indicated by algebraic decay  $r^{-n}$ . We extract the peaks from  $g(r)$ , and plot them with fits to both exponential and algebraic decay functions in figure 3. At densities higher than 0.74, exponential decay clearly underestimates correlations at large  $r/\ell$ . At the two lowest densities shown ( $\rho = 0.69, 0.70$ ), the power law overestimates the correlations, which have a pronounced downward curvature over all  $r$ . It is difficult to unambiguously identify a transition density; however, from examination of quality of fits, our best estimate for the transition from short-range to quasi-long-range translational order is  $\rho \approx 0.74$ .

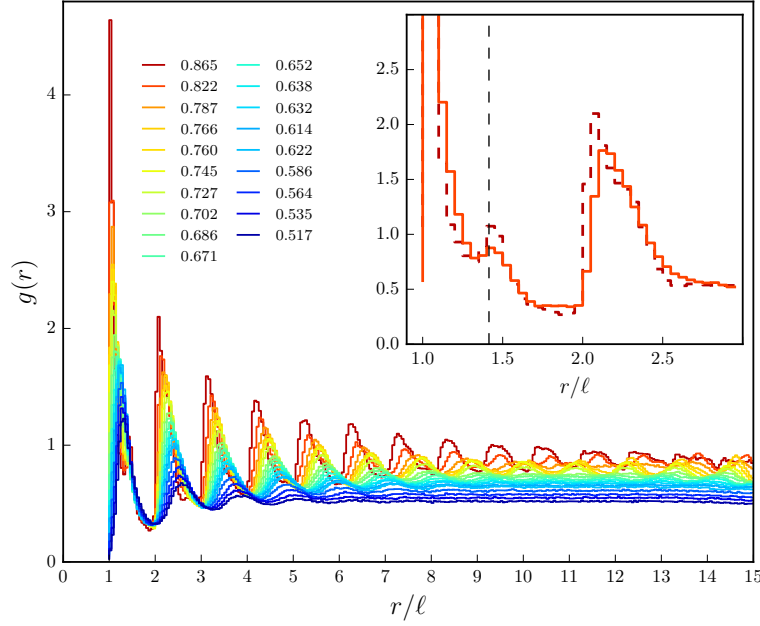


**Figure 2.**  $g(r)$ : The radial distribution function  $g(r)$  is plotted at various densities. The spatial range of translational order increases with density. Inset: Closeup of the first two peaks for highest densities. Small peaks at  $r = \sqrt{2}$  show the emergence of square-crystalline order at densities  $\rho \gtrsim 0.8$ .

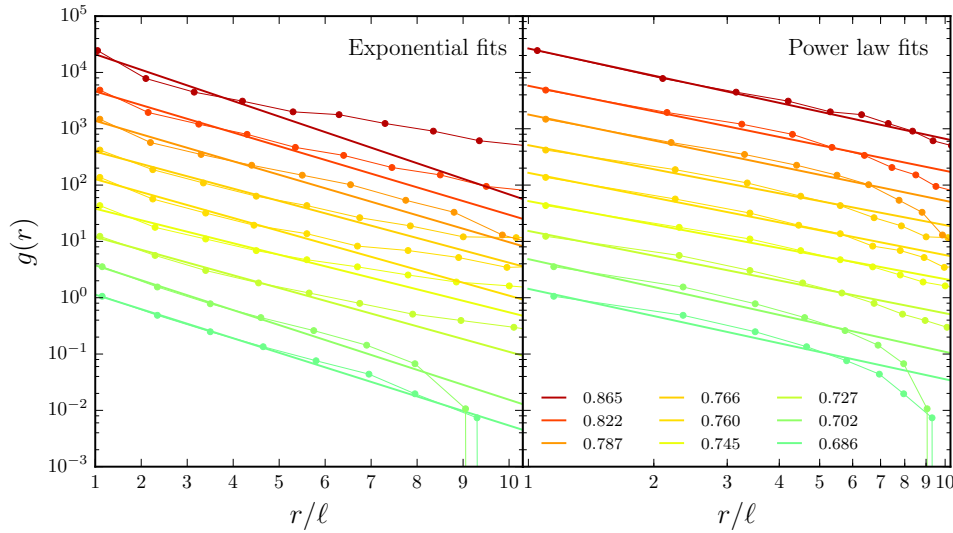


**Figure 3.** Fits to  $g(r)$ : The decay shape of the peak envelope for  $g(r)$  shows the extent of translational order. Shown are the peaks from  $g(r)$  for densities in the range 0.68 to 0.86 with fits to exponential (left) and power-law (right) decay functions. Curves of different density are vertically offset by a factor of 3 for clarity; the lowest curve has no offset.

A subtler form of spatial ordering can be studied by measuring the angles of the “bonds” connecting the centers of pairs of neighboring particles. (The bond angle  $\theta_{jk}$  does not depend on the orientation of individual particles, as illustrated in the inset diagram in figure 4, left). The global bond orientation order parameter measures  $m$ -fold lattice orientation symmetry, and is given by:

$$\Psi_m = \left| \langle e^{im\theta_{jk}} \rangle_{jk} \right|$$

where  $\theta_{jk}$  is the bond angle of neighboring particles  $j$  and  $k$ . The average is calculated over all neighboring pairs; for  $m = 4$ , neighbors are the four nearest particles, and for  $m = 6$ , neighbors are given by the Delaunay triangulation.  $\Psi_m$  are shown in figure 4 (left). We find that  $\Psi_6$  remains near zero for all densities, indicating the absence of hexagonal order; thus the hexagonal rotator phase [19] is not found for hard squares. On the other hand,  $\Psi_4$  shows a marked increase in square symmetry as density increases.

The measurements above, which depend only on the center-of-mass position of the particles, indicate the onset of translational order beginning with the condensing of inter-particle distances for  $\rho \gtrsim 0.74$ , and four-fold arrangement of particle centers. Alone, these do not uniquely distinguish the phase of anisotropic particles, as they lack information on the orientations of particles. Alignment of particle orientations, in the absence of translational order, would indicate the presence of a (tetratic, if four-fold) liquid-crystalline phase. In the next section, we report global orientational order, followed by a discussion of spatial correlations of both positional and orientational order.

### 3.2. Particle Orientational Order

The “molecular” orientation of the individual particles is given by the angle  $\gamma_i$  of the tile, illustrated in the inset diagram in figure 4 (right). Global orientational order of the system is given by the particle orientation order parameter:

$$\Phi_m = \left| \langle e^{im\gamma_i} \rangle_i \right|$$

where  $m = 4$  is the rotational symmetry and the average is taken over all particles  $i$ .

We find that  $\Phi_4$  begins increasing above the noise near density  $0.62 \pm 0.01$  (figure 4, right). This indicates an increase in global tetratic (four-fold orientational) order, analogous to nematic (two-fold) order. The bond-order  $\Psi_4$  appears at a similar density but increases more slowly, suggesting that the ordering here is primarily orientational.

A different, local measure of orientational alignment is the distribution of orientation differences between neighboring particles, as defined through a Delaunay triangulation. The width of this distribution is the normalized standard deviation of these angle differences:

$$\Delta_m = 1 - \frac{\sqrt{12}}{\pi/2} \sqrt{\langle (\delta\gamma_{ij})^2 \rangle_{\{i,j\}}}$$

where  $\delta\gamma_{ij}$  is the smallest angle between the orientations (measured modulo  $2\pi/m$ ) of neighboring particles  $i$  and  $j$ , and the average is over all such pairs. The values of  $\Delta_4$

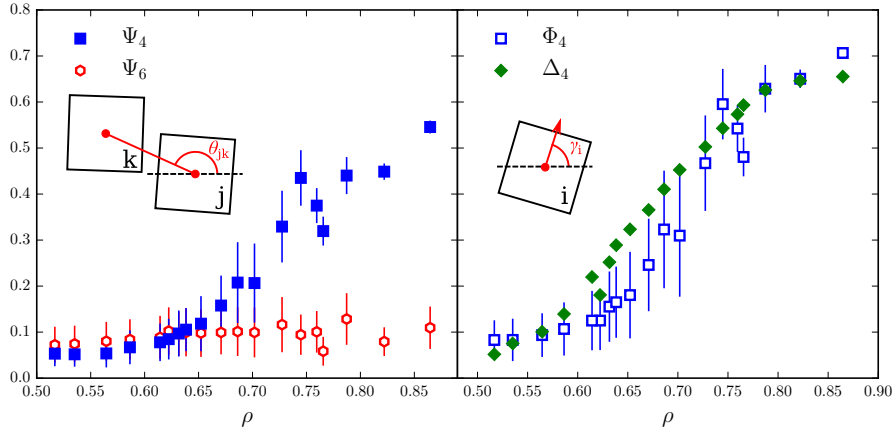


**Figure 4.** Order Parameters. Left: The bond orientation order parameter  $\Psi_m$  for both  $m = 4$  and  $m = 6$ . Inset diagram shows the bond angle  $\theta$ . We see a clear increase in four-fold bond angle ordering with none for six-fold order, indicating an approach toward square crystalline order with no evidence for the hexagonal rotator phase at any density. Right: The particle orientation order parameters  $\Phi_4$  and  $\Delta_4$ . Inset diagram shows the particle orientation angle  $\gamma$ . Both parameters show an increase in four-fold particle orientation (tetratic) order, indicating a phase with stronger orientational order than translational order.

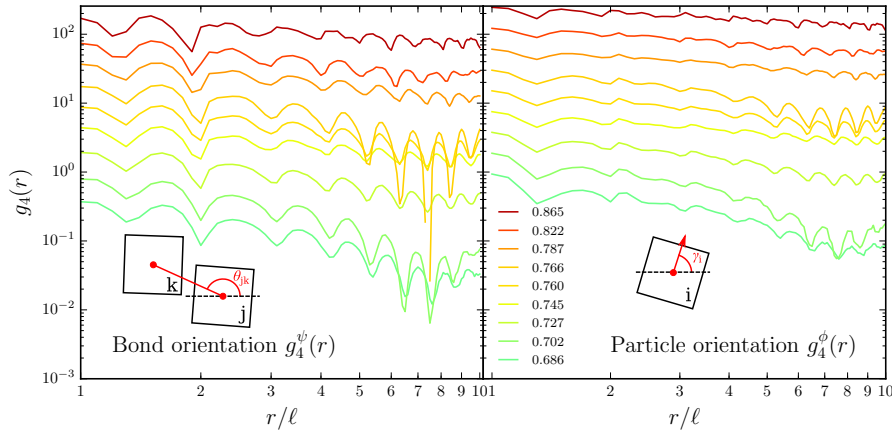


**Figure 5.** Correlation functions: The correlation functions for bond orientation  $g_m^\psi(r)$  (left) and particle orientation  $g_m^\phi(r)$  (right) for densities in the range 0.72 to 0.86. Curves of different density are vertically offset by a factor of 2 for clarity; the lowest curve has no offset. We find that bond orientation correlation has a lower amplitude and decays more quickly than the particle orientation correlation.

agree with the global orientational parameter  $\Phi_4$  as shown in figure 4, reflecting the concurrent emergence of local and global orientational alignment.

We measure the spatial extent of the above types of order by computing the associated correlation functions. The form of the decay of each correlation function allows us to distinguish between short-range order and quasi-long-range order; the former is characterized by exponential decay and the latter by algebraic decay.

The extent of particle orientational order is described by:

$$g_m^\phi(r) = \langle \cos m(\gamma_i - \gamma_j) \rangle_{r_{ij}=r}$$

where the average is taken over all pairs separated by distance  $r$ . Our data is shown in figure 5, left. We find that exponential fits underestimate the correlation for densities above  $\rho \approx 0.70$ .

We compare this to the correlation function for the bond orientational order parameter  $\psi_m$ , given by:

$$g_m^\psi(r) = \langle \psi_m^*(r_j) \psi_m(r_k) \rangle_{r_{ij}=r}$$

Here  $\psi_m(r_i)$  is the bond-orientational order parameter calculated for the neighbors of particle  $i$ . The average is taken over all pairs separated by distance  $r$ . The form of this correlation (figure 5, right) matches that of  $g^\phi(r)$ , but has lower amplitude, consistent with the respective order parameters. We observe significantly smaller oscillations in  $g^\phi(r)$  compared with  $g^\psi(r)$ . This indicates that orientational order is robust with respect to position, while bond order depends on the positional order seen in  $g(r)$ .

#### 4. Dynamics

The rotational and translational dynamics of particles reflect the constraints imposed by the spatial order in a phase. Tracking the locations of particles gives us their displacements as a function of time, from which we compute the mean squared displacement:

$$\Delta \vec{x}^2(t) = \left\langle [\vec{x}_i(t_0 + t) - \vec{x}_i(t_0)]^2 \right\rangle_{t_0, i}$$

where the average is taken over initial times  $t_0$  and all particles  $i$ . Similarly, the angular displacement of individual particles describes their average rotational motion, and is obtained by tracking the change in orientation of tiles over time:

$$\Delta \theta^2(t) = \left\langle [\theta_i(t_0 + t) - \theta_i(t_0)]^2 \right\rangle_{t_0, i}$$

From each mean squared displacement, translational and rotational, we obtain the coefficients of diffusion  $D_T$  and  $D_R$  by fitting a power law of the form  $Dt$  to the data within the diffusive regime (figures 6 and 7). As density is increased, diffusion is slowed by collisions with neighboring particles. Both coefficients decrease with increasing density, as shown in the plots of  $1/D$  in the insets of figures 6 and 7. At higher densities, particles become caged for short times and show a sub-diffusive regime before the long-time behavior becomes diffusive.<sup>†</sup>

To investigate the difference between translational and orientational order, we compare  $D_T$  and  $D_R$ . The rotational diffusion slows near  $\rho \approx 0.62$ , earlier than the translational diffusion near  $\rho \approx 0.67$ , demonstrating a freezing of orientation before that of translation. This can be seen more clearly in the decreasing ratio  $D_R/D_T$  above  $\rho \approx 0.55$ , shown in figure 8. Thus the onset of order constrains rotation at lower densities than it constrains translation.

<sup>†</sup> At very long times, we observe super-diffusive behavior, which results from a weak preference for one direction or the other in some particles. Rotation is unbiased averaged over all particles.



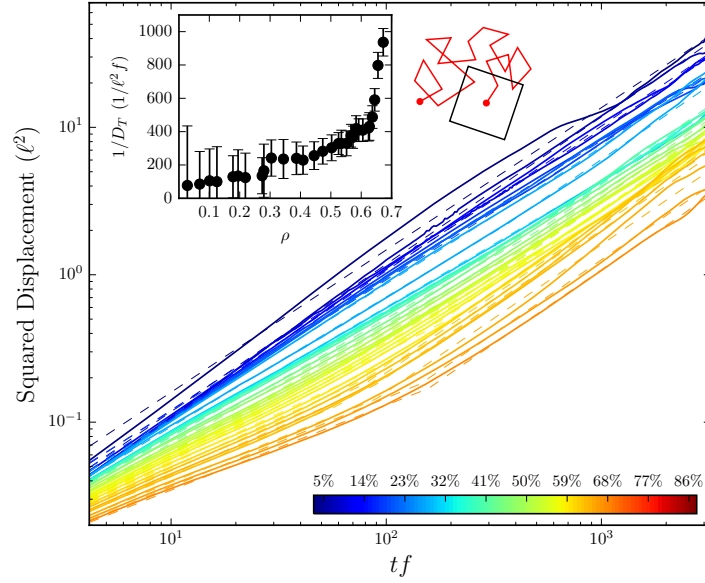


**Figure 6.** Mean Squared Displacement (in units of particle size  $\ell$ ) versus time (in units of vibration periods  $1/f$ ). Particle motion at densities ranging from 0.03 to 0.70 shows diffusive behavior at low densities with a decreasing coefficient of diffusion. At densities above 0.30, motion is not diffusive at short times, becoming diffusive only after a period of approximately 2–3 seconds. Inverse Coefficient of Diffusion (inset): Fits for coefficient of diffusion  $D_T$  are made to data for  $tf > 500$ .

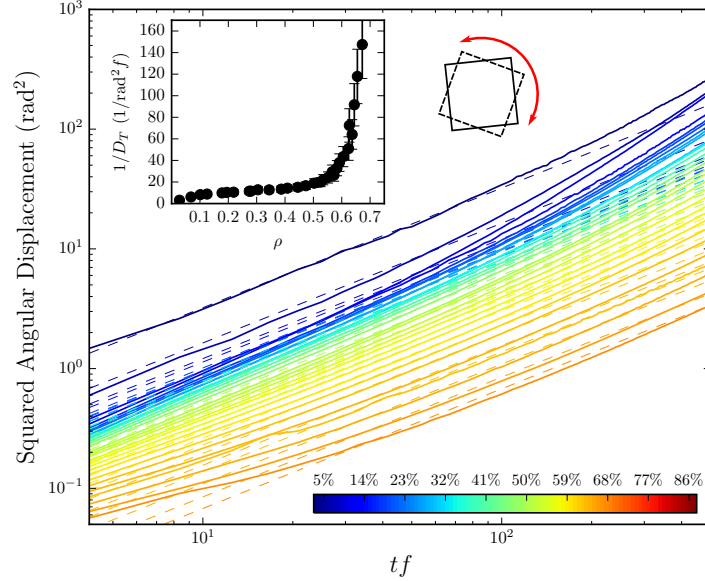


**Figure 7.** Mean Squared Angular Displacement, with time shown in units of vibration periods  $1/f$ . Particle motion at densities ranging from 0.03 to 0.70 shows diffusive behavior at low densities with a decreasing coefficient of diffusion. The mean squared angular displacement is diffusive at short times, but at long times rotational motion is super-diffusive. Inverse Coefficient of Angular Diffusion (inset): Fits for coefficient of angular diffusion  $D_R$  are made to data for  $tf < 100$ .

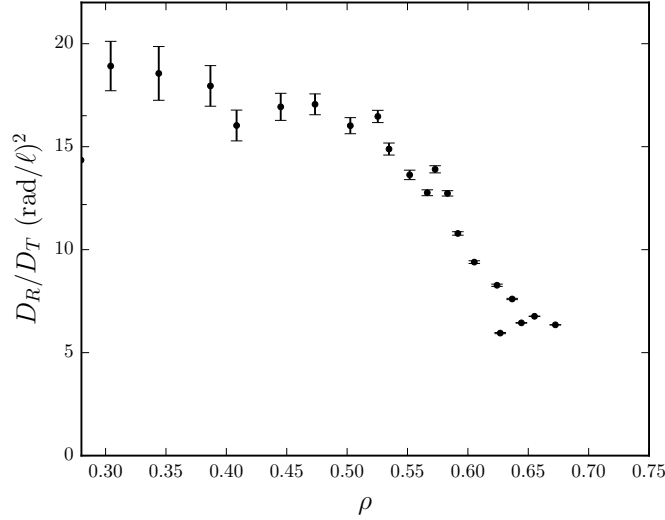


**Figure 8.** Ratio of Translational and Angular Coefficients of Diffusion: The strong decrease in  $D_R/D_T$  from density 0.50 to 0.65, shows a relative freezing of rotation compared with translation.

## 5. Conclusion

In our system of vibrated hard squares, increasing density gives rise to an increasing degree of order in the particle positions and orientations. At low density, packings are positionally and orientationally isotropic. Increasing density first leads to tetratic orientational order in the range  $\rho \approx 0.70$  to  $0.74$ . This phase is characterized by quasi-long-range, four-fold order in particle orientation with short-range translational order. With further increases in density, beyond  $\rho \approx 0.75$ , the system tends toward a quasi-long-range translationally ordered square phase. No evidence is found for hexagonal positional order at any density.

Bond-orientations, which are determined by particle positions alone, increase in the density range where tetratic orientational ordering sets in, though with smaller amplitude and shorter range. Though these are distinct kinds of order, they appear to be coupled because of the steric constraints on packing aligned particles at high densities.

To our knowledge, this is the first experimental approach to the hard-square limit. This granular system thus displays a sequence of phases consistent with equilibrium Monte Carlo simulations reported in [12] and [18]. As in those studies, the limited system size restricts structural analysis and smooths out transitions, making it difficult to pinpoint transition densities or study critical behaviour. However, measurements of the dynamics of the system — inaccessible by Monte Carlo — strengthen the evidence for the sequence of phases. The sharper decrease of rotational and translational dynamics provide additional support for the sequence of phases identified from spatial information. In particular, the ratio of translational and rotational diffusion constants is potentially a broadly useful tool to distinguish the onset of orientational and positional order.

### 5.1. Acknowledgements

We wish to thank JL Machta and JD Paulsen for helpful suggestions and conversations. This work was supported by NSF-DMR 1207778 and 1506750.

### 5.2. References

- [1] Kosterlitz J M and Thouless D J, *Ordering, metastability and phase transitions in two-dimensional systems*, 1973 *J. Phys. C: Solid State Phys.* **6** 1181
- [2] Nelson D and Halperin B, *Dislocation-mediated melting in two dimensions*, 1979 *Phys. Rev. B* **19** 2457–84
- [3] Young A, *Melting and the vector Coulomb gas in two dimensions*, 1979 *Phys. Rev. B* **19** 1855–66
- [4] Donev A, Burton J, Stillinger F and Torquato S, *Tetratic order in the phase behavior of a hard-rectangle system*, 2006 *Phys. Rev. B* **73** 054109
- [5] Zhao K, Harrison C, Huse D, Russel W B and Chaikin P M, *Nematic and almost-tetratic phases of colloidal rectangles*, 2007 *Phys. Rev. E* **76** 040401
- [6] Cuesta J A and Frenkel D, *Monte carlo simulation of two-dimensional hard ellipses*, 1990 *Phys. Rev. A* **42** 2126–36
- [7] Bates M and Frenkel D, *Phase behavior of two-dimensional hard rod fluids*, 2000 *J. Chem. Phys.* **112** 10034–41
- [8] Narayan V, Menon N and Ramaswamy S, *Nonequilibrium steady states in a vibrated-rod monolayer: tetratic, nematic, and smectic correlations*, 2006 *J Stat Mech* **2006** P01005
- [9] Müller T, Heras D de las, Rehberg I and Huang K, *Ordering in granular-rod monolayers driven far from thermodynamic equilibrium*, 2015 *Phys. Rev. E* **91** 062207
- [10] Geng J and Selinger J V, *Theory and simulation of two-dimensional nematic and tetratic phases*, 2009 *Phys. Rev. E* **80** 011707
- [11] Martínez-Ratón Y and Velasco E, *Enhanced stability of the tetratic phase due to clustering*, 2009 *Phys. Rev. E* **79** 011711
- [12] Avendaño C and Escobedo F A, *Phase behavior of rounded hard-squares*, 2012 *Soft Matter* **8** 4675–81
- [13] Martínez-Ratón Y, Velasco E and Mederos L, *Effect of particle geometry on phase transitions in two-dimensional liquid crystals*, 2005 *J. Chem. Phys.* **122**
- [14] Jiao Y, Stillinger F H and Torquato S, *Optimal packings of superdisks and the role of symmetry*, 2008 *Phys. Rev. Lett.* **100** 245504
- [15] Rossi L, Soni V, Ashton D J, Pine D J, Philipse A P, Chaikin P M, Dijkstra M, Sacanna S and Irvine W T M, *Shape-sensitive crystallization in colloidal superball fluids*, 2015 *PNAS* **112** 5286–90
- [16] Batten R D, Stillinger F H and Torquato S, *Phase behavior of colloidal superballs: Shape interpolation from spheres to cubes*, 2010 *Phys. Rev. E* **81** 061105

- [17] Damasceno P F, Engel M and Glotzer S C, *Crystalline assemblies and densest packings of a family of truncated tetrahedra and the role of directional entropic forces*, 2012 *ACS Nano* **6** 609–14
- [18] Wojciechowski K W and Frenkel D, *Tetratic phase in the planar hard square system?*, 2004 *Comput. Methods* **10** 235–55
- [19] Zhao K, Bruinsma R and Mason T G, *Entropic crystal-crystal transitions of Brownian squares*, 2011 *PNAS* **108** 2684–7
- [20] Reis P, Ingale R and Shattuck M, *Crystallization of a Quasi-Two-Dimensional Granular Fluid*, 2006 *Phys. Rev. Lett.* **96** 258001
- [21] Galanis J, Harries D, Sackett D, Losert W and Nossal R, *Spontaneous Patterning of Confined Granular Rods*, 2006 *Phys. Rev. Lett.* **96** 028002
- [22] Umbanhowar P B and Swinney H L, *Wavelength scaling and square/stripe and grain mobility transitions in vertically oscillated granular layers*, 2000 *Physica A* **288** 344–62